






 Cite this: *RSC Adv.*, 2020, 10, 2437

# Spray coated perylenebisimide/polymer film with controllable molecular aggregation state and emission properties†

 Rui Yang,  ‡<sup>a</sup> Zhijia Hu,  ‡<sup>ab</sup> Yaxin Li,<sup>b</sup> Jiangying Xia,<sup>b</sup> Jiajun Ma  \*<sup>a</sup>  
 and Junxiao Yang  \*<sup>a</sup>

Dye doped organic thin films with controllable molecular aggregation and emission properties are of broad interest to the scientific community owing to their large number of potential applications in physics, chemistry, and materials science. Here, a spray coating method was used to prepare perylenebisimides (PBI) doped polymer films. In this study, the effects of the dye concentration, polymer matrix, solvent, and casting process on the optical properties of the resulting films were studied. The aggregation of the PBI into monomer, dimer, and oligomer forms, was rapidly and simply controlled based on the concentration dependence of PBI. The molecular aggregation mechanism in the film forming process for PBI doped polystyrene (PS) was further analyzed by computer simulations. The blends rapidly reached their lowest Gibbs free energy owing to the “frozen” polymer chains and confinement of PBI, molecules with different aggregation states. Therefore, the PBIs/PS films prepared under different conditions had different fluorescent lifetimes and absolute quantum yields. Narrow emission, amplified spontaneous emission (ASE) and random lasing (RL) were observed in PBI doped PS films when photo-pumped at 532 nm in transmittance and waveguide modes, respectively. A lower ASE and RL threshold were obtained for PS films doped with monomeric PBI than those in other aggregation states. Moreover, the solvent use in film deposition greatly influenced the emission properties of the PS films by altering their microstructures. These results indicate potential applications for spray coated dye/polymer films in organic solid-state lasers.

 Received 28th November 2019  
 Accepted 2nd January 2020

DOI: 10.1039/c9ra09950f

[rsc.li/rsc-advances](http://rsc.li/rsc-advances)

## Introduction

Dyes and pigments offer many advantages for the development of novel electronic and photonic devices including ease of fabrication, mechanical flexibility, low processing temperatures, compatibility with plastic substrates, and/or high area coverage at low cost.<sup>1</sup> The performance of these materials as charge or energy transport materials depends not only on optimizing the electronic properties of the individual molecules, but also on favorable intermolecular interactions, such as  $\pi$ -stacking and hydrogen bonding to assemble larger functional structures.<sup>2</sup>

Among these materials, perylenebisimides (PBI) and their derivatives have been a subject of intense research for many

years because of their unique molecular structure with a rigid planar structure and conjugated system.<sup>3</sup> When diluted in liquid solutions, PBI has outstanding properties: high thermal and photochemical stability, and a high fluorescence quantum yield, which allows them to perform as excellent luminescent materials.<sup>4</sup> However, fluorescence quenching is observed when the concentration of PBI or doping of PBI into the solid matrix is increased, which is usually associated with the formation of a polydisperse mixture of aggregates, such as dimers, trimers, and higher order oligomers.<sup>5</sup> Aggregation-caused quenching (ACQ) phenomena of PBI have drawn considerable attention owing to intrinsic  $\pi$ - $\pi$  stacking interactions between perylene backbones.<sup>6</sup> This characteristic has been used to develop fluorescence sensing based on tuning the fluorescence to environmental stimulus.<sup>7</sup> Furthermore, intermolecular PBIs stacking can be used to form supramolecular aggregates, such as n-type organic semiconductors.<sup>8</sup>

Hence, different kinds of PBIs aggregations, with controllable emission properties, show potential for a range of applications in different fields.<sup>9</sup> Fluorescent dyes with such high efficiencies show promise for use as lasers, and many studies have focused on polymer films doped with dyes for obtaining optically pumped thin film organic lasers (TFOLs).<sup>10</sup> In the case

<sup>a</sup>State Key Laboratory of Environment-friendly Energy Materials, School of Material Science and Engineering, Southwest University of Science and Technology, Mianyang 621010, China. E-mail: jiajunma@yeah.net; yangjunxiao@swust.edu.cn

<sup>b</sup>School of Instrument Science and Opto-Electronics Engineering, Hefei University of Technology, Hefei, Anhui 230009, P. R. China

† Electronic supplementary information (ESI) available. See DOI: 10.1039/c9ra09950f

‡ These authors contributed equally to this work.



of PBIs doped polymer films, aggregation of PBIs molecules in the thin films [e.g., non-aggregated state (monomer), extended aggregates (dimer and oligomer), or microcrystals] influences the absorption and fluorescence wavelength, quantum yield, amplified spontaneous emission (ASE) and random lasing (RL) properties. The excitation diffusion and excited states are influenced by intermolecular interactions of the dyes and aggregate formation is also affected by features such as intermolecular distance and the conformation of polymer chains.<sup>11</sup> Hence, there is a need to understand and control the molecular aggregation state of the dye molecules in the polymer matrix.

Furthermore, the casting formation is a crucial aspect determining the device performance. Dip-coating and spin-coating are conventional and well-defined film casting processes, which are often used for casting dye doped polymer films for a wide range of applications (see Table S1 in the ESI† for characteristics of different film coating methods).<sup>11b,12</sup> The films prepared by these two traditional methods have good optical quality; however, there are inherent drawbacks, such as a limited solvent selection, poor uniformity of the film thickness, and a relatively slow deposition rate. In addition, long evaporation time for the solvents in dip-coating reduces processing efficiency and might result in heterogeneous thickness, low transparency to visible light and poor reproducibility, as shown in Fig. 1A and F. In the development of efficient film casting processes, spray coating has advantages in terms of its high uniformity and ease of operation. For this reason, spray coating has been used in solar cells, super-hydrophobic coatings and metal processing (see in Table S1 in ESI†).<sup>13</sup> Moreover, spray coating generates small droplets in the micrometer range and can be used to deposit films over large areas on a variety of substrates, including planar and non-planar surfaces and meshes, with excellent reproducibility.<sup>14</sup> Therefore, spray

coating shows considerable potential as a technology for exploring interactions between dyes and polymer chains in TFOLs.

In this work, spray coating performed to obtain PBI (hexylheptyl-PBI, as shown in Fig. 1B and C for the chemical structure and optimized structure) doped polymer (polystyrene (PS) and polymethylmethacrylate (PMMA), as shown in Fig. 1D and E for the chemical structure) films with uniform thickness, controllable roughness, high orange-red light transparency, and excellent reproducibility. The spray coated PBIs/polymer films were more smooth and uniform than a film prepared by conventional dip-coating method (Fig. 1A, F and G). The optical properties of the hexylheptyl-PBI in the polymer film cast by spray-coating and the interactions between the dye molecules and polymers were investigated. We controlled the molecular aggregation state through the concentration dependence of hexylheptyl-PBI in the polymer films and performed an in-depth study on the contrast of the lasing performance in different aggregation states. Importantly, spray-coating was used for the first time as a method of film casting in the study of molecular aggregation stage and emission properties of PBI-doped polymer films.

## Experimental

### Materials

Chemicals and solvents were used for the synthesis of *N,N'*-di-(1-hexylheptyl) perylene-3,4,9,10-tetracarboxylic-7-tridecanone (97.0%, TCI, Tokyo, Japan), sodium cyanoborohydride (97.0%, Energy Chemical, Shanghai, China), ammonium acetate (97.0%, Energy Chemical, Shanghai, China), hydrochloric acid (HCl, 35%, KeLong Chemical Reagent Co., Ltd., Chengdu, China), methanol (MeOH, 99.5%, KeLong Chemical Reagent

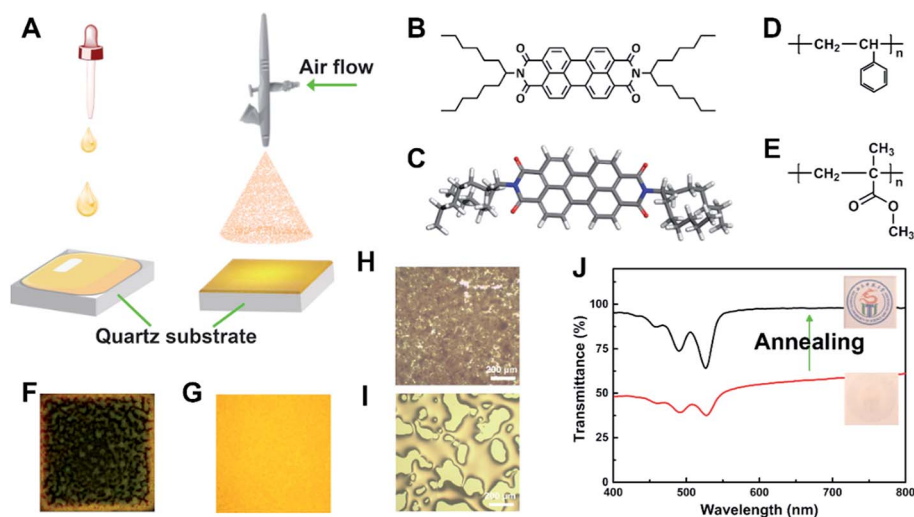


Fig. 1 (A) Schematic representation of setup for dip-coating and spray-coating; (B) molecular structure of *N,N'*-di-(1-hexylheptyl) perylene-3,4,9,10-tetracarboxylic bisimide (hexylheptyl-PBI); (C) optimized structure of hexylheptyl-PBI; (D) and (E) chemical structure of PS and PMMA, respectively. (F) and (G) fluorescent images (under 365 nm UV lamp) of hexylheptyl-PBI/PS thin films prepared by dip-coating and spray-coating, respectively; (H) and (I) optical micro-images of spray coated PS films before and after annealing, respectively; (J) transmittance of spray coated PS films before and after annealing, respectively.



Co., Ltd., Chengdu, China), 3,4,9,10-perylenetetracarboxylic dianhydride (98.0%, Energy Chemical, Shanghai, China), dichloromethane ( $\text{CH}_2\text{Cl}_2$ , 99.5%, Energy Chemical, Shanghai, China). All chemicals and solvents were used without further purification, except for  $\text{CH}_2\text{Cl}_2$ .  $\text{CH}_2\text{Cl}_2$  was used after drying by molecular sieve 4A (2–3 nm off-white powder, Adamas, Shanghai, China) overnight. Hexylheptyl-PBI was synthesized by reacting PDI with 1-hexylheptylamine following synthetic procedures reported previously,<sup>15</sup> with  $^1\text{H}$  NMR spectra seen in Fig. S1.† PS (average  $M_w = 260 \text{ kg mol}^{-1}$  by GPC, J&K Chemical, Santiago, USA) and PMMA (average  $M_w = 350 \text{ kg mol}^{-1}$  by GPC, Sigma-Aldrich Inc., St. Louis, USA) were used without further purification. Solvents were used for spray coating and dip coating: tetrahydrofuran (THF, 99.8%, KeLong Chemical Reagent Co., Ltd., Chengdu, China), toluene (99.8%, KeLong Chemical Reagent Co., Ltd., Chengdu, China), carbon disulphide ( $\text{CS}_2$ , 99.9%, KeLong Chemical Reagent Co., Ltd., Chengdu, China), trichloromethane ( $\text{CHCl}_3$ , 99.0%, KeLong Chemical Reagent Co., Ltd., Chengdu, China), which were used after drying by molecular sieve 4A overnight. Quartz substrates ( $1.5 \text{ cm} \times 1.5 \text{ cm}$ , Purshee Optical Elements. Co., Ltd, Yixing, China) were immersed in ethanol (EtOH, 99.5%, KeLong Chemical Reagent Co., Ltd., Chengdu, China) and sonicated for 30 min in a bath sonicator (ultrasonic cleaner SK2200H, 100 W, 53 kHz, Kedao Ultrasound Instrument Co., Ltd., Shanghai, China). After the glass sides were washed in deionized water, they were cleaned by heating ( $60 \text{ }^\circ\text{C}$ ) in a mixture of 70% concentrated  $\text{H}_2\text{SO}_4$  (98.0%, KeLong Chemical Reagent Co., Ltd., Chengdu, China) and 30%  $\text{H}_2\text{O}_2$  (35.0%, KeLong Chemical Reagent Co., Ltd., Chengdu, China) (7 : 3 v/v) for 2 h. And then they were thoroughly rinsed with deionized water and ethanol, the glass sides were dried by air flow.

### Spray coated method

The spray-coating was operated with a Battery Mini Air Compressor (HS08 Serries, Haosheng Pneumatic Machinery Co., Ltd., NingBo, China) equipped with an AccuMist atomizing nozzle (Sono-Tek Corp., Auburn Hills, USA). The operation diagram is shown in Fig. 1A, and this film formation was compared with traditional dip-coating technology, which was operated by desktop spin coater (CHY-EZ4, Henan Chengyi Equipment Science and Technology Ltd., Zhengzhou, China) with the speed of 800 rpm for 180 s.

Firstly, hexylheptyl-PBI was dissolved into THF to obtain a stock solution with different dye concentrations. Secondly, PS or PMMA were added to the stock solution with different polymer concentrations, followed by stirring overnight until full dissolved at room temperature, respectively. Thirdly, the hexylheptyl-PBI/polymer THF solution was then placed in a syringe pump connected by tubing to the nozzle with the diameter of 0.2 mm. The distance between nozzle and quartz substrate was 13 cm. The pump was programmed to a constant air flow rate of  $0.1 \text{ mL min}^{-1}$  and a steady working pressure of 15 psi. The indoor temperature was controlled at about  $20 \pm 5 \text{ }^\circ\text{C}$  when spraying.

Spray coating process can be described from the microscopic point: (1) generation of fine droplets (atomisation); (2) impingement on the surface (deposition); (3) coalescence of droplets on the substrate (coalescence).<sup>16</sup> After that, the films show very poor optical transmittance (as shown in Fig. 1H and J). Therefore, the films were further thermally annealed on a hotplate, rising from room temperature to  $200 \text{ }^\circ\text{C}$ , and maintaining at this temperature for 0.5 h. Finally, the transparent dye doped polymer film (as shown in Fig. 1J, the transmittance around 550–600 nm has been greatly improved after annealing) with the thickness of  $6.1 \text{ }\mu\text{m}$  ( $20.0 \text{ }\mu\text{m}$  before annealing) was obtained after cooling to room temperature. In addition, spraying-coated films were prepared with different solvents (chloroform, THF, toluene and  $\text{CS}_2$ ) under same experiment conditions, the thickness of films after thermal annealing were measured, as shown in Table S2 (in ESI†), solvents cause little effect on the thickness of spraying-coated films. However, the fluorescent intensity of dye/PS film by using  $\text{CS}_2$  as solvent is low than that of THF before or after annealing (see Fig. S2 in ESI†).

In the experiment, we adjusted the concentration of dye (hexylheptyl-PBI doped concentration: C1–C6 = 0.19, 0.38, 0.95, 1.9, 3.8, 11.4 wt% of polymer) and polymer (polymer concentration: 20, 25, 30, 35, 40  $\text{mg mL}^{-1}$ ), respectively. Besides, the effects of organic solvents (THF, toluene,  $\text{CS}_2$  and  $\text{CHCl}_3$ ) on the optical properties were detail studied in our experiments.

### Characterization

$^1\text{H}$  NMR spectra were recorded in  $\text{CDCl}_3$  on a Bruker NMR spectrometer (Avance 600, Rheinstetten, Germany), using tetramethylsilane (TMS) as an internal reference. Film thickness was measured by means of an interferometer coupled to a Bruker optical microscope (DEKTAK XT, Karlsruhe, Germany). Absorption and transmission spectra were measured on a Shimadzu UV-Vis-NIR spectrophotometer (Solidspec-3700, Kyoto, Japan). Emission spectra were measured on a Hitachi fluorescence spectrophotometer (F-4500, Tokyo, Japan). X-ray diffractometer (XRD) patterns were recorded on a Malvern Panalytical X-ray diffractometer (X'Pert Pro, Almero, Netherlands) with  $\text{Cu-K}\alpha$  radiation. Surface topography of film was recorded on an optical microscope (XPN-203E, Changfang Optical Instruments Co., Ltd, Shanghai, China). Fluorescence attenuation spectra of film sample with the peak value of maximum absorption wavelength as excitation light, as well as absolute quantum yield (QY%) of film sample, were tested on time-resolved fluorescence spectrometer (FLS920, Edinburgh Instrument Co., Ltd., Livingston, UK).

Laser pump experiments were measured on the setup for film samples: a Q-switched Nd:YAG laser (Q-smart 850, Quantel, France), which has an output wavelength of 532 nm with a round spots (pulse duration of 10 ns, repetition rate of 10 Hz), is used to end pump the different types of samples. A Glan prism group is used to control the pump laser energy and polarization. Ophir pump pulse energy (Vega, Littleton, USA) is used to measure the pump laser energy. A filter for 532 nm is placed behind the samples to filter the residual pump pulse.



The emitted light is collected by an Ocean Optics fiber spectrometer (QE65PRO, Winter Park, USA) with resolution of 0.4 nm and integration time of 100 ms. As shown in Fig. 5A and 6A, the emission is collected with transmission mode and waveguide mode, respectively. All experimental trials were carried out at room temperature (295 K).

Computer simulations were performed to study the optimized models and total energy of PBI/THF, PS/THF and PBI/PS blends using BIOVIA Materials Studio (2017, Accelrys Inc., San Diego, USA). Full atomic models of PS, THF and PBI were constructed using Material Visualizer module in Material Studio software. Molecule models were optimized by Forcite module (COMPASSII force field) in the software, the energy convergence threshold of  $1 \times 10^{-4}$  kcal mol<sup>-1</sup> and the force convergence of 0.005 kcal mol<sup>-1</sup> Å<sup>-1</sup>. The atom-based summation was applied for the van der Waals interactions with a cut-off distance of 9.5 Å, a spline width of 1 Å, and a buffer width of 0.5 Å. When blends module was used to calculate PBI/THF, PS/THF and PBI/PS systems, PS and THF were set as base role, PS and PBI were set as screen role.

## Results and discussion

Hexylheptyl-PBI was synthesized in Kim's work by a two-step route for use as an intermediate product to obtain the brush polymer (PacPDI).<sup>15</sup> PacPDI can self-assemble into  $\pi$ -stacked aggregates through thermal annealing and displays high performance n-type unipolar volatile memory behavior.<sup>15</sup> In this work, hexylheptyl-PBI was used as a laser dye to study molecular aggregation state and emission properties, particularly when doped into polymer films.

Absorption spectra of a hexylheptyl-PBI/THF solution were measured at room temperature by varying the concentrations of the dye from  $2.5 \times 10^{-6}$  M to  $7.5 \times 10^{-5}$  M, as seen in Fig. 2A. The electronic absorption spectra obviously contained main bands with maxima at 523, 485, 455, and 425 nm, which correspond to  $\pi$ - $\pi^*$  transitions from the electronic ground state (S<sub>0</sub>) to different vibrational levels (0-0, 0-1, 0-2, and 0-3) of the first electronic excited state (S<sub>1</sub>).<sup>17</sup> Fig. 2B shows classical specular symmetry between the sharp, well-resolved fluorescence spectra of dye/THF solution and absorption spectra with peaks at 537, 576, and 627 nm. As the energy loss of excited state caused by vibration relaxation, the fluorescence spectrum is located at a higher wavelength (lower energy) than the absorption spectrum.<sup>18</sup> The wavenumbers between the maximum of the first absorption band and the maximum of fluorescence, 14 nm, is the Stokes shift.

As shown in Fig. 1C, as the concentration of hexylheptyl-PBI was increased, the wavelength corresponding to the maximum of absorption peak (at 523 nm) changed very little. The relationship between the absorbance and concentration was linear up to  $C_{\text{PBI}} = 50 \mu\text{M}$ , and subsequently, the absorption increased less rapidly. For further increases of concentration, the fluorescence emission spectra first increased and then decreased, before reaching a maximum value between 10–25  $\mu\text{M}$ . Furthermore, the wavelength for the peak at 537 nm started to slightly red shift at  $C_{\text{PBI}} > 10 \mu\text{M}$ . This shift suggests the

formation of aggregates by intermolecular  $\pi$ - $\pi$  interactions, referred to as a head-to-tail arrangement (*i.e.*, J-aggregates) of PBI molecules.<sup>19</sup>

After annealing, the hexylheptyl-PBI/PS films changed from opaque to transparent (Fig. 1J), the transmittance of the films decreased with increasing film thickness (Fig. S3 in ESI<sup>†</sup>), and the absorption and fluorescence spectra of the films changed at different dye concentrations. As shown in Fig. 2D and E, at a low dye concentration, the absorption peak decreased after annealing; however, the position of the peak did not change. A similar tendency was found in the fluorescence spectra at this concentration. At high dye concentrations, the emission spectra of the corresponding film were characterized by a considerable blue-shift from 617 to 608 nm after annealing. This blue shift indicates weakening of the aggregation or a tendency for the molecules to switch to a parallel arrangement during contraction of polymer chains, this aggregation-inhibited process is similar to that of QDs embedding in a 1D polymer by electro-spinning method.<sup>20</sup> Notably, the fluorescent intensity before annealing was greater than that after annealing in Fig. 2E, which is attributed to the reflection of the rough surface of the opaque film. In addition, the peak shape of the dye/PS films in different concentrations is also different (illustration in Fig. 2E). When hexylheptyl-PBI was doped into PMMA, both absorption (see Fig. S4 in ESI<sup>†</sup>) and fluorescence spectra (Fig. 2F) showed molecular changes: the transition from the aggregated state to the monomer state. Thus, the annealing process further weakened the aggregation rather than inducing molecular rearrangement of hexylheptyl-PBI molecules.

Fig. 3A illustrates the UV-Vis absorption spectra of hexylheptyl-PBI/PS films at concentration of C1 and C5. Absorption spectra of PBIs are sensitive to the inter-distance and orientation and therefore have been widely used to study their  $\pi$ - $\pi$  stacking.<sup>21</sup> A small red-shift in the absorption bands was observed at higher wavelengths (461 and 492 nm) compared with their respective solution spectra (455 and 485 nm). Such effects might be a consequence of molecular J-aggregates in the films.<sup>19</sup> However, the hexylheptyl-PBI/PMMA film showed a greater red shift of the absorption spectra than that of hexylheptyl-PBI/PS film at the same concentration (C1 and C5, see in Fig. S2 in ESI<sup>†</sup>). Fig. 3B and C show the fluorescent emission spectra of different dye concentrations of hexylheptyl-PBI in PS and PMMA films, respectively. The relative emission intensities between PS and PMMA were clearly different, which might be attributed to the compatibility of hexylheptyl-PBI in two polymers. At the lower concentrations of samples C1 and C2 (for PS) and sample C1 (for PMMA), structural fluorescent bands appeared at 535, 574, and 621 nm, and their spectral shape was the same as those observed in solution, which corresponds to the emission spectra of monomeric PBI.<sup>19a,22</sup> Fluorescent intensity at both 574 and 621 nm increased for C3 (for PS) and C2–C4 (for PMMA), where the main form of the molecules was stacked dimers or the extended aggregates.<sup>23</sup> The observed decrease of the 535 nm band upon increasing the dye concentration might be attributed to reabsorption of the fluorescence or energy transfer to the broad fluorescence band located within the longer wavelength region.<sup>24</sup> The 621 nm peak red-shifted as



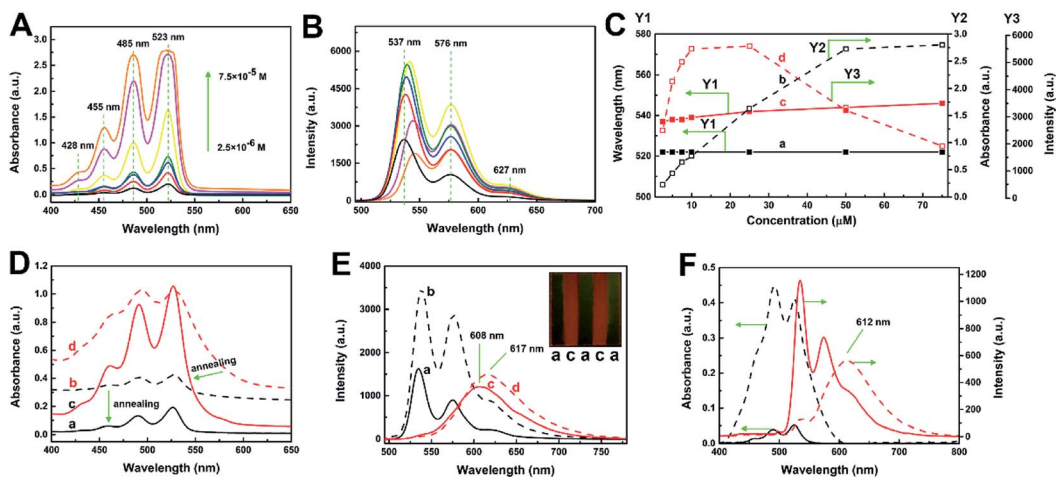


Fig. 2 Absorption spectra (A) and fluorescence emission spectra (B) of hexylheptyl-PBI/THF solution by varying the molar concentration. (C) Variation of the spectral information with the change of dye concentration: the wavelength of the maximum absorption peak (black solid with solid point), the wavelength of the maximum fluorescent peak (red solid with solid point), the intensity of the maximum absorption peak (black dotted lines with hollow point) and the intensity of the maximum fluorescent peak (red dotted lines with hollow point). Absorption spectra (D) of hexylheptyl-PBI/PS film: before (b: black dotted lines) and after (a: black lines) annealing with low dye concentration; before (d: red dotted lines) and after (c: red lines) annealing with high dye concentration. Fluorescent spectra (E) of hexylheptyl-PBI/PS films before (dotted lines) and after (solid lines) annealing with low dye concentration (a and b) and high dye concentration (c and d); insets are photographs showing fluorescence of the films under ultraviolet light. (F) Absorption spectra (black line) and fluorescence emission spectra (red line) of hexylheptyl-PBI/PMMA film with low dye concentration (solid lines) and high dye concentration (dotted lines) after annealing.

the concentration was further increased, eventually extending to 627 nm at C6. At the same time, the fluorescent intensity decreased, which suggested that excimer emission and/or energy transfer to oligomeric sites effectively occurred at high

concentrations.<sup>23</sup> Additionally, emission of hexylheptyl-PBI in the PS matrix red-shifts was less than 8 nm compared with that of the dye/PMMA film. When hexylheptyl-PBI was excited in the PMMA matrix, the excitation was released in a non-radiative

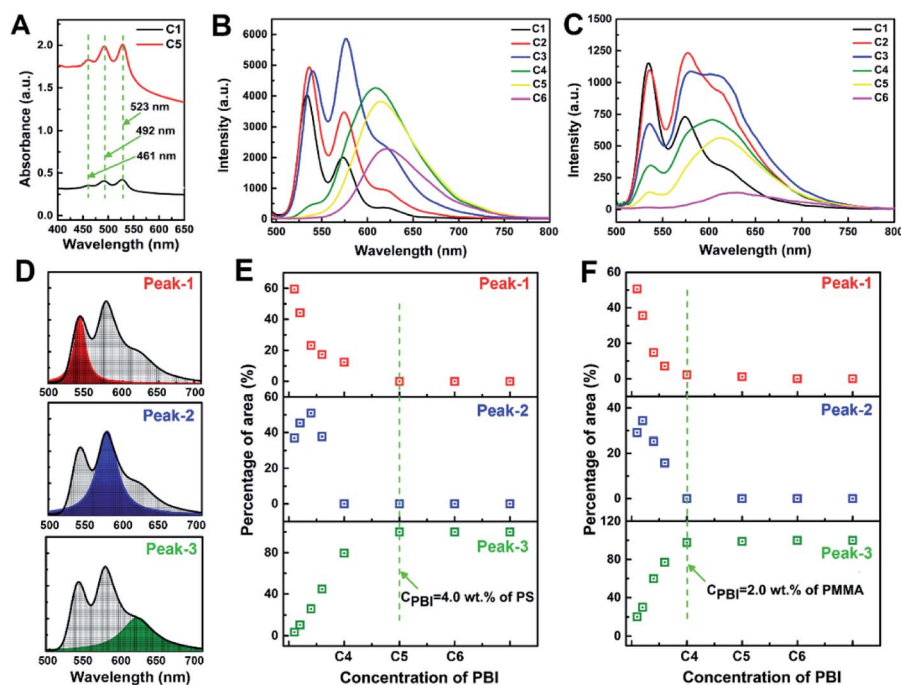


Fig. 3 (A) Absorption spectra of hexylheptyl-PBI/PS with the concentration of C1 and C5. Fluorescence emission spectra of different dye concentrations of hexylheptyl-PBI in PS (B) and PMMA (C) films, respectively. (D) Spectral area of 535 nm (Peak-1, red area), 574 nm (Peak-2, blue area) and 621 nm (Peak-3, green area). Contribution of Peak-1, Peak-2, and Peak-3 to total peak area, versus concentration of hexylheptyl-PBI in PS (E) and PMMA thin films (F).



manner, which contributed to the lower fluorescent intensity of the dye/PMMA film.<sup>12</sup> In addition, the emission peak shifted red and the fluorescence intensity decreased with the increase of annealing temperature (Fig. S5 in ESI†). It was possibly due to the collision probability between dye–dye and dye–polymer molecules, increase of temperature caused the excess vibration energy was released as non-radiation transitions, and finally led to the weakening of fluorescence intensity and the red shift of fluorescence spectrum.

As previously reported, molecular aggregation may correlate with the peak area.<sup>25</sup> As shown in Fig. 3D and E for hexylheptyl-PBI/PS films, the area ratio of peak at 535 nm (Peak-1) has a downward trend and decreases to 0 at C5, suggesting that the 0–0 vibronic progression was disrupted, which was caused by the transformation from monomer to dimer. The peak at 621 nm (Peak-3) showed the opposite trend. Notably, the curve of the peak at 574 nm (Peak-2) of hexylheptyl-PBI/PS thin films increased and then decreased to 0 when the concentration approaches that of sample C4. In the hexylheptyl-PBI/PMMA films, Peak-3 reached 100% at C4 whereas Peak-1 and Peak-2 were absent. A possible reason for the increase of Peak-3 is the shorter dye intermolecular distance at higher concentrations. The concentration dependence of the hexylheptyl-PBI/PMMA film followed the same trend as that of the dye/PS film; however, aggregation of the dye occurred at lower dye concentrations in the PMMA than PS matrix. Hence, PMMA induced the dye molecules to transform into dimers and promoted aggregate formation at lower concentrations. The miscibility between the dye molecules and polymer is an important factor in controlling the dispersion within the film.

Absorption and fluorescence spectra of hexylheptyl-PBI/PS films with various concentrations of polymer showed clear effects on the absorbance and emission intensity. As shown in Fig. S6A–C (in ESI†), the film's absorbance decreased as the mass fraction of PS decreased with increasing dye concentration in samples C1, C3, and C5. This result is explained by dilution of the dye in the polymer matrix. The changes of the fluorescent intensity in monomer state (Fig. S6A in ESI,† C = C1) were consistent with those of the absorption spectra. These results are attributed to the dye intermolecular distance being determined by the polymer chains. Thus, for dimers with slightly stronger aggregation, the mass fraction of PS shows the less effect on the decrease of fluorescent intensity (Fig. S6B in ESI,† C = C3). In addition, the fluorescent intensity first decreased and then increased at the dye concentration of sample C5 (oligomeric state, Fig. S6C in ESI†). The former effect relates to dilution of the aggregates whereas the latter relates to restriction of macromolecular chains on aggregation behavior.

As shown in Fig. 4A and B, in the process of spray-coating, most of the solvent was rapidly removed and subsequently droplets of dye/polymer solution were deposited onto the quartz substrate. After annealing, the films further shrank through complete volatilization of the organic solvent. Combined with Fig. 1D and E, the annealing process caused a weak blue shift of the emission peaks, rather than red-shifting and the ACQ effect. During deposition, the rapid “freezing” of the polymer chains confined the dyes to their lowest Gibbs free energy to form

greater aggregation.<sup>20</sup> The annealing process caused PBI molecules to dissolve into the PS matrix and disaggregated at the same time. In Fig. 4C–E, the hexylheptyl-PBI and PS blend had the lowest binding energies. Thus, the PS molecular chains have good compatibility with the dyes. XRD data also showed that there was no phase separation between the PS and dye (see in Fig. S7 in ESI†). Therefore, the aggregation state was simply and rapidly controlled in a uniform PS or PMMA film by controlling the concentration of dyes (see in Fig. S8 and S9 in ESI†).

The dye/PS film was filled with small particles before annealing for all the three aggregated states; and the films become flat and the particles become large after annealing, as shown in Fig. S10 (in ESI†). To further demonstrate the fluorescence properties of hexylheptyl-PBI in the monomer and aggregate forms, time-resolved fluorescence measurements were performed (see in Fig. S11 in ESI†). The fluorescence of dye in the PS film in monomeric, dimeric, and oligomeric states were fitted by single exponential functions, giving a single fluorescence lifetime (4.2, 17.3, and 23.1 ns, respectively). Thus, the lifetimes of the dimer and oligomers were respectively 18.9 and 5.8 ns, higher than that of monomer form. Furthermore, monomeric hexylheptyl-PBI in PS film shows a high absolute quantum yield of 65.98%, as shown in Fig. S12 (in ESI†); however, this value decreases as the concentration of dye increased in the PS film. The quantum yields were 65.12% and 50.94% for the dimeric and oligomeric hexylheptyl-PBI, respectively. The above results are unlike those of Kaiser and coworker's reports: for monomers in solution, lifetimes of 6.5–7.3 ns were obtained, whereas aggregates in solution had considerably smaller values of 2.1–2.7 ns.<sup>26</sup> In our experiments, the prolonged lifetimes and decreased quantum yield at a high dye concentration in the PS film are attributed to monomer transfer to the aggregates.<sup>27</sup> The emission properties of the aggregates were similar to the “excimer-type” emission. In fact, the term “excimer-type” exhibited three characteristic features of an excimer (*i.e.*, unstructured, longer-lived, red-shifted emission not present in the monomer).<sup>28</sup> Here, we cannot exclude the possibility that the emitting species were also bound in the ground state, one important reason for this is the distinct observed aggregate absorption.

In theory, fluorescence lifetime and fluorescence quantum yield are determined by the radiation attenuation rate ( $I$ ) and non-radiative attenuation rate ( $k_{nr}$ ). According to a Jablonski energy level diagram, for fluorescent molecules in the free-state in the absence of other special quenching processes, their fluorescence lifetime and quantum yield are  $\tau$  and  $Q$ , respectively:<sup>29</sup>

$$\tau_0 = (I + k_{nr})^{-1},$$

$$Q_0 = I/(I + k_{nr}).$$

Hence, a higher radiative decay rate gives a shorter fluorescence lifetime and a higher quantum yield of the fluorescent molecules. For a given fluorescent molecule, changes in the environment around the fluorescent molecules (*i.e.*, media and



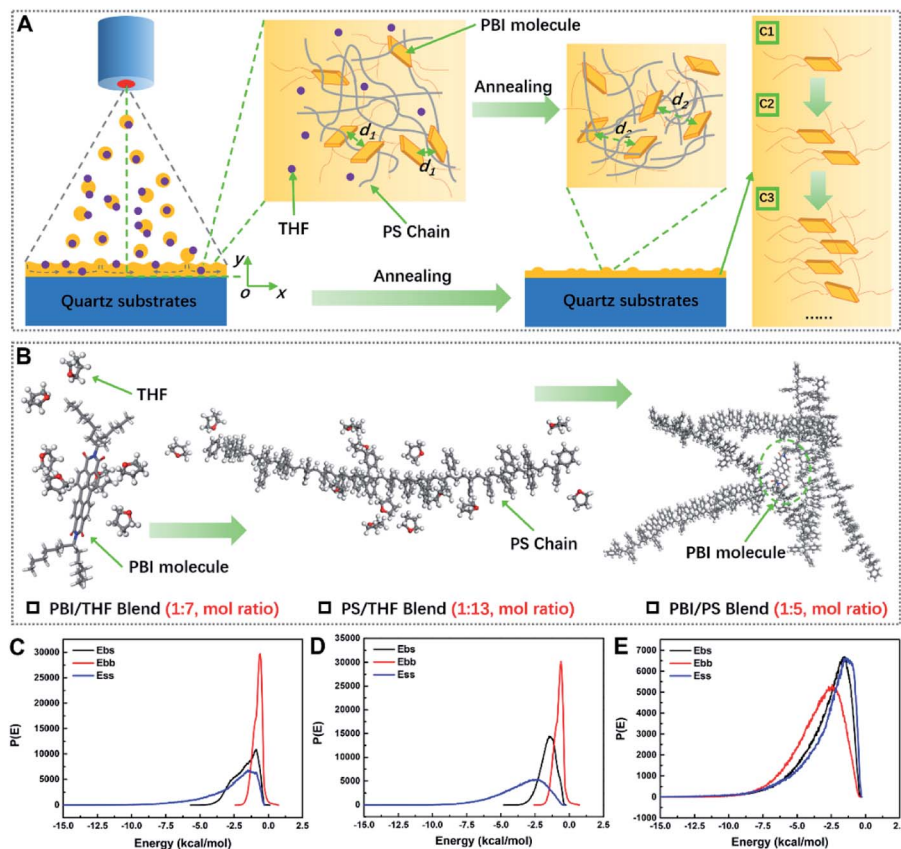


Fig. 4 Change of molecular aggregates throughout the spray-coating process (A). Blend process and molecule ratio of PBI/THF, PS/THF, and PBI/PS systems (B). Distribution of binding energies  $P(E)$  between THF and hexylheptyl-PBI (bs), THF and THF (ss), and hexylheptyl-PBI with hexylheptyl-PBI (bb); (C)  $P(E)$  between THF and PS (bs), THF and THF (ss), and PS with PS (bb); (D)  $P(E)$  between hexylheptyl-PBI and PS (bs), PS and PS (ss), and hexylheptyl-PBI with hexylheptyl-PBI (bb) (E), results simulated by BIOVIA Materials Studio.

molecular aggregation) affect the fluorescence lifetime and fluorescence intensity, and these changes in turn affect  $\Gamma$  and  $k_{nr}$ . Therefore, according to the formula,  $\Gamma$  was calculated to be 0.157, 0.038, and 0.022 ns<sup>-1</sup> for monomeric, dimeric and oligomeric hexylheptyl-PBI, whereas  $k_{nr}$  was calculated to be 0.081, 0.02, and 0.02 ns<sup>-1</sup> for monomeric, dimeric and oligomeric dye. The calculated values of  $\Gamma$  and  $k_{nr}$  were of the same order of magnitude, which indicated that both  $\Gamma$  and  $k_{nr}$  influenced the emission properties of the hexylheptyl-PBI/PS film. In addition, according to the principle of quantum electrodynamics, the spontaneous emission rate of photons is the radiation decay rate of excited states.<sup>30</sup> Therefore, a relatively large  $\Gamma$  and  $k_{nr}$  value of the monomeric hexylheptyl-PBI/PS film might suggest stimulated emission properties.

Films doped with hexylheptyl-PBI were photo-pumped at 532 nm to identify the presence of stimulated emission, as shown in Fig. 5A for the transmission mode. Fig. S13 (see in ESI†) shows the evolution of the emission spectra for hexylheptyl-PBI in a PS film as the pump energy increased. At low power, the spectra showed broad emission: the peak intensity was low and the full width at half maximum (FWHM) was large, owing to spontaneous emission of the hexylheptyl-PBI/PS film, as seen in Fig. 5B. As the pump energy was increased the FWHM became narrower and the peak intensity

increased. The emission peak became narrower at 578 nm owing to preferential amplification at frequencies close to the maximum of the gain spectra. This phenomenon shows that the stimulated emission of the hexylheptyl-PBI/PS film under intense light pumping occurs in the gain region, that is, amplified spontaneous emission (ASE).<sup>23,31</sup> In addition, the linewidth of the lasing peak was 3–4.5 nm for the dye/PS film. As Fig. 5B shows, the ASE wavelength corresponds to the wavelength of the S0–S1 transition of the fluorescent spectra. It should be noted that the ASE positions remain unaltered in the aggregated state of the dye in the PS films, although the shape of the fluorescent spectra and the peak positions varied together with the concentration. This is an indication that the energy levels involved in the laser transitions are related to those of the monomeric and dimeric PBI units rather than those of oligomeric aggregates, which emit at longer wavelengths. The photostability of the hexylheptyl-PBI/PS film was also studied by recording the total ASE intensity emitted as a function of the number of pump pulses (*i.e.*, times), by keeping a constant pump intensity (see Fig. 5C). These results indicate that hexylheptyl-PBI has excellent luminous stability in the aggregation state.

The threshold of the films doped with hexylheptyl-PBI was also studied by recording the total ASE intensity emitted as



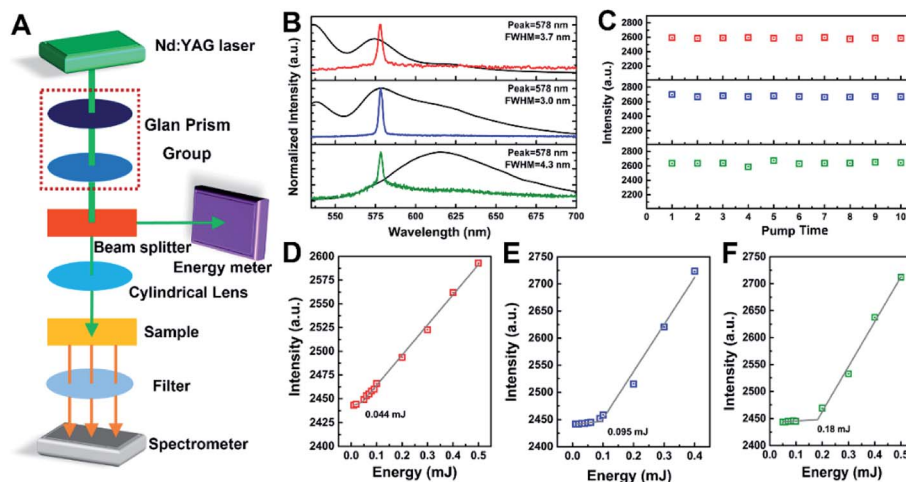


Fig. 5 (A) Schematic diagram for testing the emission properties by transmission mode. (B) Spontaneous emission (black lines, fluorescence) and stimulated emission (color lines, ASE) of hexylheptyl-PBI/PS film with different molecular aggregated states (red line: monomeric PBI, blue line: dimeric PBI and green line: oligomeric PBI), photo-pumped at 532 nm; (C) the ASE photostability of hexylheptyl-PBI/PS film with different molecular aggregated state (red line: monomeric PBI, blue line: dimeric PBI and green line: oligomeric PBI); (D and E) total ASE intensity emitted as a function of pump energy, a threshold behavior was observed for monomeric (D), dimeric (E) and oligomeric (F) dye.

a function of pump energy, which was observed at 0.044, 0.095, and 0.18 mJ for the monomeric (D), dimeric (E), and oligomeric (F) dyes, respectively, as shown in Fig. 5D–F. Under a weak pumping energy, the molecules of the gain medium in the hexylheptyl-PBI/PS films undergo a spontaneous transition, and output anisotropic fluorescence. However, the hexylheptyl-PBI/PS films are a kind of asymmetric planar optical waveguide structure. Stimulated emission of the dye/PS films is not only related to the molecular structure of the gain material, but also to the optical waveguide mode transmission. The organic waveguide film is composed of three layers of dielectrics. The substrate is a quartz substrate, the guided wave layer is a PS organic film, and the covering layer is air. The refractive indexes of the three layers are 1.4499, 1.5905, and 1, respectively. According to optical waveguide theory, the total reflection angle of light waves at the upper interface of the waveguide is greater than that at the lower interface, and light waves can be transmitted by total reflection in the waveguide layer to form a guided mode; otherwise, the light wave will overflow the waveguide from the upper interface or the lower interface. Therefore, when the pump spot is perpendicular (*i.e.*,  $\theta = 90^\circ$ ) to the film surface, the stimulated radiation wave satisfies the guided mode relationship and was transmitted in the film.

As shown in Fig. 6A and B for testing the emission properties by waveguide mode, at low pump energy, the output spectrum of the film was a broad-band spontaneous emission spectrum with a peak at 578 nm. When the pump energy exceeded the threshold value of 239.95  $\mu\text{J}$ , there were several discrete peaks in the original flat broad spectrum. This stimulated emission phenomenon, is quite different from the ASE of hexylheptyl-PBI/PS films, but similar to reported “random laser” phenomenon in our previous works.<sup>32</sup> According to the theory of random lasers, light waves are scattered by disorder structures in random gain thin films (Fig. 6F), and it is possible to return to

the original scattered particles and form a closed loop. Under the waveguide effect of light waves, the closed loop can provide coherent feedback for transmitting light waves and generate random lasing when the gain of the light wave is large (Fig. 6G). For the sprayed hexylheptyl-PBI/PS films, the rough morphology (Fig. 6D(a–c)) and polymer/dye particles (Fig. 6E(e–h)) constituted a disorder gain body. However, it is difficult to observe random lasers in transmission mode even if the pumping capacity is improved. One explanation might be that the lack of waveguide and thus the random gain of thin films is poor. Hu *et al.* confirmed that the waveguide effect can boost coherent RL emission.<sup>33</sup> In addition, for dimeric and oligomeric dye/PS films, ASE is the main form of emission in both transmission and waveguide modes.

The evaporation rate of the solvent greatly influences the physical and/or mechanical properties of polymers by changing their microstructures. Comparing the optical microscope images (Fig. 6D and E) and 3D topography (Fig. S14 in ESI†) before and after annealing, the difference in film roughness was clearly visible to the naked eye. Most of the defects in the films were eliminated by thermal annealing, and the films became flat and uniform (Fig. 1J). However, the annealing process caused a large number of microscopic defects (air cavities and polymer/dye particles) inside the film during the spray-coating process, as shown in Fig. 6D and E. In fact, random lasing is based on the existence of defects that act as scatters in combination with fluorescent monomeric hexylheptyl-PBI that serves as a gain medium. Notably, for the sample based on  $\text{CHCl}_3$  as the spraying solvent (Fig. 6D and J), air cavities disappeared owing to solvent evaporation during spraying and successive annealing, the separated peaks attached to the spectral lines disappeared and the output spectral lines were smooth. Obviously, emission being scattered only by polymer/dye particles indicated incoherent random lasing. As a result, the emission





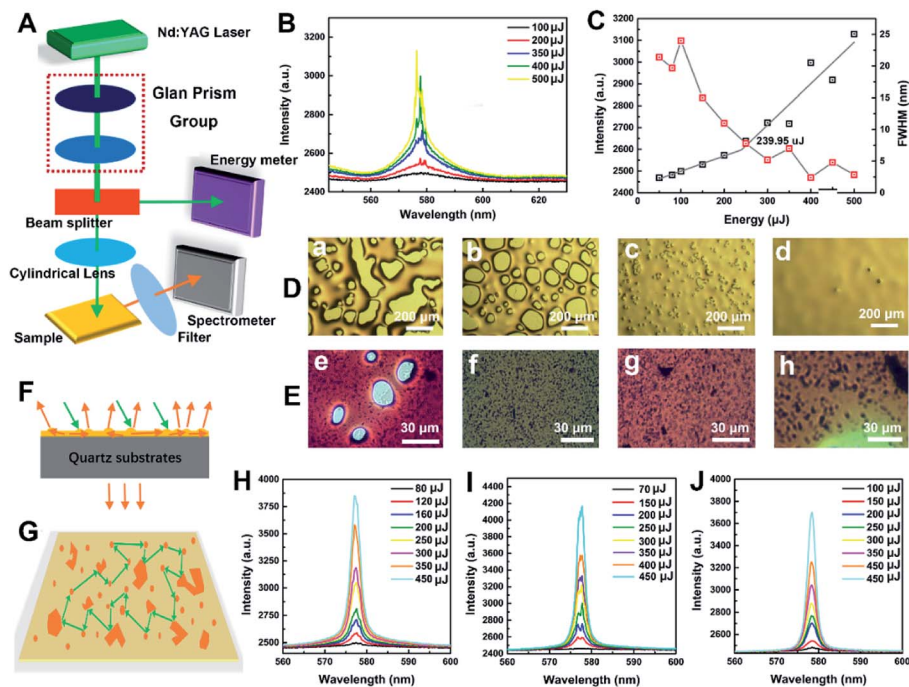


**Fig. 6** (A) Schematic diagram of setup used to measure the emission properties by waveguide mode. (B) Emission spectra of hexylheptyl-PBI/PS film at different pump pulse energies. (C) Integrated intensity (black line) and linewidth of emission peak (red line) of hexylheptyl-PBI/PS film as a function of pump power. Different morphologies (D and E) of hexylheptyl-PBI/PS film with varying spraying solvent conditions. (a and e: THF; b and f: toluene; c and g: CS<sub>2</sub>; d and h: chloroform). Waveguide and scattering diagram of light in hexylheptyl-PBI/PS film (F) and coherent feedback for transmitting light wave in hexylheptyl-PBI/PS film (G). Emission spectra of hexylheptyl-PBI/PS film at different pump pulse energies with varying spraying solvent conditions ((H) toluene; (I) CS<sub>2</sub>; (J) chloroform).

intensity was not able to soar significantly when the pump intensity increased.

Combined with the advantages of spray coating technology, the as-deposited dye/polymer film, generate new phenomena and realize new function, which has potential applications in the photonics field. In the preparation of light emitting diode (LED), white LED can be obtained by fast layer-by-layer spray coating with controllable molecular aggregation state. The spray coated film can be simple fixed into non-planar surface of optical fiber and different grating structure to prepare optical sensor with color, absorbance, fluorescence, ASE, RLs as the response signal. The unique emission properties of dye-doped polymer films can be also used as the fluorescent waveguide for luminescent solar concentrator. These will be gradually carried out in our future works.

## Conclusions

Here, spray coating was performed to obtain hexylheptyl-PBI doped polymer (PS and PMMA) films. By analysis of the UV-Vis absorbance and fluorescent spectra in solution and films, the aggregation state of PBIs, containing monomer, dimer and oligomer, was rapidly and simply controlled by taking advantage of the concentration dependence of PBIs. The annealing process after spray coating improves the transmittance around 550–600 nm, simultaneously, obviously happens to disaggregate. The molecular aggregated mechanism in the film forming

process for PBI doped PS was further analyzed by computer simulation, which showed that the blends rapidly reached their lowest Gibbs free energy owing to the “frozen” polymer chains and confined PBI molecules. Time-resolved fluorescence and absolute quantum yield measurements confirmed that the prolonged lifetimes and decreased quantum yield upon increasing concentration of dye in PS film are attributed to monomer transfer to the aggregates. Narrowed emission, ASE, and RL were observed in PBI doped PS films when photo-pumped at 532 nm at the transmitting and waveguide mode, respectively. The stable and lowest threshold ASE was obtained for PS films doped with monomeric PBI at the transmitting mode, although ASE positions remained essentially unchanged for dye in the aggregated state of the dye in the PS film. Under the waveguide mode for PS films doped with monomeric PBI, the waveguide effect of the light wave and the closed network provide coherent feedback for transmitting light waves and generate RL when the pump energy exceeded the threshold value of 239.95 μJ. In addition, the solvent greatly influenced the emission properties of the dye/PS films by affecting their microstructures. As the films became smoother and the number of particles in the film decreased, the number of peaks decreased. Thus, the emission properties of the thin films changed from RL to ASE at the same emission intensity. In our experiments, hexylheptyl-PBI was used as an activating material with good gain characteristics in the spray coated polymer film. Controllable emission properties, low threshold ASE and RL



were obtained in the controlled molecular aggregation state. Therefore, we provide a new approach to designing solid-state thin-film lasers with excellent performance.

## Conflicts of interest

There are no conflicts to declare.

## Acknowledgements

This work was financially supported by National Nature Science Foundation of China (51603173) and the Project of State Key Laboratory of Environment-friendly Energy Materials, Southwest University of Science and Technology (No. 17FKSY0102, 18FKSY0206 and 19FKSY11). We thank the China Academy of Physics Engineering for their support of computer simulation.

## Notes and references

- (a) M. Gsänger, D. Bialas, L. Huang, M. Stolte and F. Würthner, *Adv. Mater.*, 2016, **28**, 3615–3645; (b) M. Freitag, J. Teuscher, Y. Saygili, X. Zhang, F. Giordano, P. Liska, J. Hua, S. M. Zakeeruddin, J.-E. Moser, M. Grätzel and A. Hagfeldt, *Nat. Photonics*, 2017, **11**, 372–378; (c) D. Joly, P.-A. Bouit and M. Hissler, *J. Mater. Chem. C*, 2016, **4**, 3686–3698; (d) Y. X. Li, S. S. Wang, L. Z. Jin, X. H. Ding, C. J. Ou, Y. Wei, R. Rong, L. H. Xie and W. Huang, *Cryst. Growth Des.*, 2018, **18**, 4822–4828; (e) M. N. Yu, H. Soleimaninejad, J. Y. Lin, Z. Y. Zuo, B. Liu, Y. F. Bo, L. B. Bai, Y. M. Han, T. A. Smith, M. Xu, X. P. Wu, D. E. Dunstan, R. D. Xia, L. H. Xie, D. D. C. Bradley and W. Huang, *J. Phys. Chem. Lett.*, 2018, **9**, 364–372.
- (a) M. N. Yu, J. Y. Lin, Y. X. Li, H. Soleimaninejad, C. J. Ou, L. B. Bai, B. Liu, W. Liu, Q. Wei, Y. F. Bo, T. A. Smith, D. E. Dunstan, K. P. Ghiggino, L. H. Xie, C. X. Xu, D. D. C. Bradley and W. Huang, *Chem*, 2019, **5**, 2470–2483; (b) F. Würthner, *Acc. Chem. Res.*, 2016, **49**, 868–876; (c) S. Herbst, B. Soberats, P. Leowanawat, M. Stolte, M. Lehmann and F. Würthner, *Nat. Commun.*, 2018, **9**, 2046; (d) Q. Li, C. Shi, M. Huang, X. Wei, H. Yan, C. Yang and A. Yuan, *Chem. Sci.*, 2019, **10**, 3257–3263; (e) Z. Y. Zuo, C. J. Ou, Y. J. Ding, H. Zhang, S. X. Sun, L. H. Xie, R. D. Xia and W. Huang, *J. Mater. Chem. C*, 2018, **6**, 4501–4507.
- (a) L. Chen, C. Li and K. Müllen, *J. Mater. Chem. C*, 2014, **2**, 1938–1956; (b) T. Weil, T. Vosch, J. Hofkens, K. Peneva and K. Müllen, *Angew. Chem., Int. Ed. Engl.*, 2010, **49**, 9068–9093.
- (a) Z. Chen, U. Baumeister, C. Tschierske and F. Würthner, *Chem.–Eur. J.*, 2007, **13**, 450–465; (b) Z. Chen, A. Lohr, C. R. Saha-Möller and F. Würthner, *Chem. Soc. Rev.*, 2009, **38**, 564–584; (c) A. Liscio, G. D. Luca, F. Nolde, V. Palermo, K. Müllen and P. Samorì, *J. Am. Chem. Soc.*, 2008, **130**, 780–781; (d) L. Schmidt-Mende, A. Fechtenkötter, K. Müllen, R. H. Friend and J. D. MacKenzie, *Phys. E*, 2002, **14**, 263–267.
- J. Mizuguchi and K. Tojo, *J. Phys. Chem. B*, 2002, **106**, 767–772.
- S. W. Eaton, L. E. Shoer, S. D. Karlen, S. M. Dyar, E. A. Margulies, B. S. Veldkamp, C. Ramanan, D. A. Hartzler, S. Savikhin, T. J. Marks and M. R. Wasielewski, *J. Am. Chem. Soc.*, 2013, **135**, 14701–14712.
- (a) Y. B. Ruan, A. F. Li, J. S. Zhao, J. S. Shen and Y. B. Jiang, *Chem. Commun.*, 2010, **46**, 4938–4940; (b) Z. Chen, M. G. Debije, T. Debaerdemaeker, P. Osswald and F. Würthner, *Chemphyschem*, 2004, **5**, 137–140.
- F. Würthner and M. Stolte, *Chem. Commun.*, 2011, **47**, 5109–5115.
- (a) J. K. Gallaher, E. J. Aitken, R. A. Keyzers and J. M. Hodgkiss, *Chem. Commun.*, 2012, **48**, 7961–7963; (b) B. P. Jiang, D. S. Guo and Y. Liu, *J. Org. Chem.*, 2010, **75**, 7258–7264; (c) V. Dehm, M. Büchner, J. Seibt, V. Engel and F. Würthner, *Chem. Sci.*, 2011, **2**, 2094–2100.
- (a) L. Cerdán, A. Costela, G. Durdán-Sampedro, I. García-Moreno, M. Calle, M. Juan-y-Seva, J. Abajob and G. A. Turnbull, *J. Mater. Chem.*, 2012, **22**, 8938–8947; (b) V. Navarro-Fuster, E. M. Calzado, P. G. Boj, J. A. Quintana, J. M. Villalvilla, M. A. Díaz-García, V. Trabadelo, A. Juarros, A. Retolaza and S. Merino, *Appl. Phys. Lett.*, 2010, **97**, 171104; (c) M. G. Ramírez, M. Morales-Vidal, V. Navarro-Fuster, P. G. Boj, J. A. Quintana, J. M. Villalvilla, A. Retolaza, S. Merino and M. A. Díaz-García, *J. Mater. Chem. C*, 2013, **1**, 1182–1191.
- (a) F. Ito and C. Kikuchi, *Bull. Chem. Soc. Jpn.*, 2017, **90**, 709–713; (b) F. Ito, K. Yamamoto, Y. Kogasaka and R. Katoh, *Langmuir*, 2018, 8b01342.
- R. Muñoz-Mármol, N. Zink-Lorre, J. M. Villalvilla, P. G. Boj, J. A. Quintana, C. Vázquez, A. Anderson, M. J. Gordon, A. Sastre-Santos, F. Fernández-Lázaro and M. A. Díaz-García, *J. Phys. Chem. C*, 2018, **122**, 24896–24906.
- (a) A. Reale, L. L. Notte, L. Salamandra, G. Polino, G. Susanna, T. M. Brown, F. Brunetti and A. D. Carlo, *Energy Technol.*, 2000, 1–23; (b) S. Das, B. Yang, G. Gu, P. C. Joshi, I. N. Ivanov, C. M. Rouleau, T. Aytug, D. B. Geohegan and K. Xiao, *ACS Photonics*, 2015, **2**, 680–686; (c) J. Li, Z. Jing, F. Zha, Y. Yang, Q. Wang and Z. Lei, *ACS Appl. Mater. Interfaces*, 2014, **6**, 8868–8877; (d) J. Li, R. Wu, Z. Jing, L. Yan, F. Zha and Z. Lei, *Langmuir*, 2015, **31**, 10702–10707.
- (a) N. P. Pham, E. Boellaard, J. N. Burghartz and P. M. Sarro, *J. Microelectromech. Syst.*, 2004, **13**, 491–499; (b) N. P. Pham, J. N. Burghartz and P. M. Sarro, *J. Micromech. Microeng.*, 2005, **15**, 691–697.
- Y. Y. Kim, B. J. Ree, M. Kido, Y. G. Ko, R. Ishige, T. Hirai, D. Wi, J. Kim, W. J. Kim, A. Takahara and M. Ree, *Adv. Electron. Mater.*, 2015, **1**, 1500197.
- S. Bose, S. S. Keller, T. S. Alstrøm, A. Boisen and K. Almdal, *Langmuir*, 2013, **29**, 6911–6919.
- (a) K. D. Belfield, M. V. Bondar, O. V. Przhonska and K. J. Schafer, *J. Photochem. Photobiol., A*, 2002, **151**, 7–11; (b) M. Adachi, Y. Murata and S. Nakamura, *J. Phys. Chem.*, 1995, **99**, 14240–14246; (c) A. Kam and R. Aroca, *Chem. Mater.*, 1998, **10**, 172–176; (d) L. B.-Å. Johansson and H. Langhals, *Spectrochim. Acta, Part A*, 1991, **47A**, 857–861.
- B. Valeur and M. N. Berberan-Santos, *Molecular Fluorescence, Encyclopedia of Applied Physics*, Wiley-VC, Weinheim, 2012.



- 19 (a) J. D. Fernandes, W. M. Pazin, R. F. Aroca, W. D. Macedo Jr, S. R. Teixeira and C. J. L. Constantino, *Spectrochim. Acta, Part A*, 2019, **211**, 221–226; (b) R. M. Hochstrasser and M. Kash, *Photochem. Photobiol.*, 1964, **3**, 317–331.
- 20 M. Li, J. Zhang, H. Zhang, Y. Liu, C. Wang, X. Xu, Y. Tang and B. Yang, *Adv. Funct. Mater.*, 2007, **17**, 3650–3656.
- 21 (a) W. Wang, L. S. Li, G. Helms, H. H. Zhou and A. D. Q. Li, *J. Am. Chem. Soc.*, 2003, **125**, 1120–1121; (b) P. M. Kazmaier and R. Hoffmann, *J. Am. Chem. Soc.*, 1994, **116**, 9684–9691; (c) K. Balakrishnan, A. Datar, R. Oitker, H. Chen, J. Zuo and L. Zang, *J. Am. Chem. Soc.*, 2005, **127**, 10496–10497; (d) K. Balakrishnan, A. Datar, T. Naddo, J. Huang, R. Oitker, M. Yen, J. Zhao and L. Zang, *J. Am. Chem. Soc.*, 2006, **128**, 7390–7398.
- 22 C. J. L. Constantino, T. Lemma, P. A. Antunes and R. Aroca, *Spectrochim. Acta, Part A*, 2002, **58**, 403–409.
- 23 J. M. Giaimo, J. V. Lockard, L. E. Sinks, A. M. Scott, T. M. Wilson and M. R. Wasielewski, *J. Phys. Chem. A*, 2008, **112**, 2322–2330.
- 24 F. Ito, Y. Kogasaka and K. Yamamoto, *J. Phys. Chem. B*, 2013, **117**, 3675–3681.
- 25 E. Yariv, S. Schultheiss, T. Saraidarov and R. Reisfeld, *Opt. Mater.*, 2001, **16**, 29–38.
- 26 T. E. Kaiser, V. Stepanenko and F. Würthner, *J. Am. Chem. Soc.*, 2009, **131**, 6719–6732.
- 27 (a) Y. Liu, K. R. Wang, D. S. Guo and B. P. Jiang, *Adv. Funct. Mater.*, 2009, **19**, 2230–2235; (b) Z. Chen, V. Stepanenko, V. Dehm, P. Prins, L. D. Siebbeles, J. Seibt, P. Marquetand, V. Engel and F. Würthner, *Chem.–Eur. J.*, 2007, **13**, 436–449.
- 28 E. E. Neuteboom, S. C. J. Meskers, E. W. Meijer and R. A. J. Janssen, *Macromol. Chem. Phys.*, 2004, **205**, 217–222.
- 29 J. R. Lakowicz, C. D. Geddes, I. Gryczynski, J. Malicka, Z. Gryczynski, K. Aslan, J. Lukomska, E. Matveeva, J. Zhang, R. Badugu and J. Huang, *J. Fluoresc.*, 2004, **14**, 425–441.
- 30 E. S. C. Ching, P. T. Leung and K. Young, *Optical Processes in Microcavities-The Role of Quasinormal Modes*, 1996, DOI: 10.1142/9789812830760\_0001.
- 31 (a) E. M. Calzado, J. M. Villalvilla, P. G. Boj, J. A. Quintana, R. Gómez, J. L. Segura and M. A. Díaz-García, *J. Phys. Chem. C*, 2007, **111**, 13595–13605; (b) E. M. Calzado, A. Retolaza, S. Merino, M. Morales-Vidal, P. G. Boj, J. A. Quintana, J. M. Villalvilla and M. A. Díaz-García, *Opt. Mater. Express*, 2017, **7**, 1295–1301; (c) Y. X. Li, H. Zhang, M. N. Yu, S. S. Wang, Y. R. Liu, D. Q. Lin, L. H. Xie, Z. Q. Lin and W. Huang, *Nanoscale*, 2019, **11**, 5158–5162.
- 32 (a) J. Xia, K. Xie, J. Ma, X. Chen, Y. Li, J. Wen, J. Chen, J. Zhang, S. Wu, X. Cheng and Z. Hu, *Nanophotonics*, 2018, **7**, 1341–1350; (b) X. Chen, K. Xie, X. Zhang, Z. Xie, J. Ma, J. Wen, J. Chen, J. Zhang, X. Cheng and Z. Hu, *Phys. Scr.*, 2019, **94**, 115509.
- 33 Z. Hu, Q. Zhang, B. Miao, Q. Fu, G. Zou, Y. Chen, Y. Luo, D. Zhang, P. Wang, H. Ming and Q. Zhang, *Phys. Rev. Lett.*, 2012, **109**, 253901.

